Feed-forward inhibition as a buffer of the neuronal input-output relation

Michele Ferrante[a], Michele Migliore[b], and Giorgio A. Ascoli[a,c,1]

[a]Krasnow Institute for Advanced Study, Center for Neural Informatics, Structures, and Plasticity, George Mason University, 4400 University Drive, MS 2A1 Fairfax, VA 22030; [b]Institute of Biophysics, National Research Council, via U. La Malfa 153, 90146 Palermo, Italy; and [c]Department of Molecular Neuroscience, Krasnow Institute for Advanced Study, George Mason University, 4400 University Drive, MS 2A1 Fairfax, VA 22030

Edited by Charles F. Stevens, The Salk Institute for Biological Studies, La Jolla, CA, and approved September 4, 2009 (received for review May 14, 2009)

Neuronal processing depends on the input-output (I/O) relation between the frequency of synaptic stimulation and the resultant axonal firing rate. The all-or-none properties of spike generation and active membrane mechanisms can make the neuronal I/O relation very steep. The ensuing nearly bimodal behavior may severely limit information coding, as minimal input fluctuations within the expected natural variability could cause neuronal output to jump between quiescence and maximum firing rate. Here, using biophysically and anatomically realistic computational models of individual neurons, we demonstrate that feed-forward inhibition, a ubiquitous mechanism in which inhibitory interneurons and their target cells are activated by the same excitatory input, can change a steeply sigmoid I/O curve into a double-sigmoid typical of buffer systems. The addition of an intermediate plateau stabilizes the spiking response over a broad dynamic range of input frequency, ensuring robust integration of noisy synaptic signals. Both the buffered firing rate and its input firing range can be independently and extensively modulated by biologically plausible changes in the weight and number of excitatory synapses on the feed-forward interneuron. By providing a soft switch between essentially digital and analog rate-code, this continuous control of the circuit I/O could dramatically increase the computational power of neuronal integration.

computational models | dentate gyrus | hippocampus | interneurons | networks

Inhibition in the cortex is mostly achieved by interneurons releasing GABA on principal cells. The interneuron axons target specific postsynaptic subdomains (perisomatic, axonic, and layer-specific dendritic shafts or spines), creating computational modules that influence the neuronal response to various spatial and temporal patterns of excitation (1). The neuronal input-output (I/O) relationship between the mean frequency of synaptic stimulation and the resulting axonal firing can be directly affected by inhibitory signals that are delivered to the same dendritic regions receiving the excitation (2). In particular, shunting inhibition modulates this rate-coded information processing both in terms of offset, or stimulus threshold (3) and of gain, or slope (4). In the cortex, however, GABAergic interneurons are morphologically, chemically, and physiologically more diverse than principal cells (5, 6). Relatively little is still known about signal integration in different inhibitory circuits and the effects on network dynamics (7).

Many cortical interneurons perform both feedback and feed-forward inhibitory functions, balancing these roles dynamically based on local and afferent activity or neuromodulation (7–10). In feed-forward inhibition (FFI) a principal cell and an interneuron receive excitatory inputs from the same presynaptic source. The interneuron then outputs its inhibitory signal to the principal cell. Thus, upon activation of the presynaptic source, the principal cell receives 2 types of input, one excitatory and one inhibitory, separated by a brief delay due to the interneuron integration. Feed-forward inhibition has been reported in a variety of cortical regions, including somatosensory (5), perirhinal (11), subicular (12), hippocampal (13), piriform (14), and cerebellar (4). This neuronal circuit may help control both spike timing in principal cells (15) and the propagation of epileptiform waves (16).

Despite this ubiquity and functional involvement in pathophysiological conditions, the specific role of FFI in shaping the neuronal I/O relationship is not yet thoroughly understood. This limited knowledge is due to the technical difficulty of controlling all experimental conditions in the intricate, dynamic, and diverse FFI circuit. Computational models can foster intuition about complex problems by requiring the precise and explicit definition of all variables and assumptions. Computer simulations cannot falsify a hypothesis, but may provide proof of concept of putative mechanisms as well as quantitative estimates of the parameter range of their applicability. We recently proposed that FFI could affect the I/O relationship above and beyond a modulation of gain and/or offset, by stabilizing the output firing rate at an intermediate value between quiescence and saturation over a range of input stimulus rates (17). The underlying idea is based on the observation that the interneuron I/O curve is itself characterized by a linear component between offset and saturation. Thus, the subtractive property of FFI can be exploited by matching the ratio between excitatory and inhibitory signals to the principal cell with the interneuron gain. In principle, the resulting balance of excitation and inhibition would result in a constant total input to the principal cell over a range of stimulation frequencies from the presynaptic source. The corresponding output would also be constant, forming an I/O buffer system analogous to that of chemical titrations (e.g., pH). Thus, FFI could accomplish the role assigned to input vector normalization in artificial neural networks.

Here, we define and explore this potential mechanism in detail using compartmental simulations of an individual granule cell and feed-forward interneuron from the rat dentate gyrus. This hippocampal region has an identified FFI component (18–20) that may modulate the I/O relationship between signals from the entorhinal cortex and granule cell responses. The interneurons of a particular GABAergic class, MOlecular layer Perforant Pathway (MOPP) cells (18), extend both their dendrites and axons through the molecular layer, thus sharing with the granule cells the perforant pathway excitation from the entorhinal cortex, and also targeting the granule cells dendrites in the same regions. The results indicate that the buffering role of FFI is compatible with plausible biophysical parameters. Moreover, the model predicts that both the buffered output firing rate and the input frequency dynamic range can be extensively and robustly modulated by the number and weights of the excitatory synapses on the FFI interneurons.

Author contributions: M.F., M.M., and G.A.A. designed research, performed research, analyzed data, and wrote the paper.

The authors declare no conflict of interest.

This article is a PNAS Direct Submission.

[1]To whom correspondence should be addressed. E-mail: ascoli@gmu.edu.

This article contains supporting information online at www.pnas.org/cgi/content/full/0904784106/DCSupplemental.

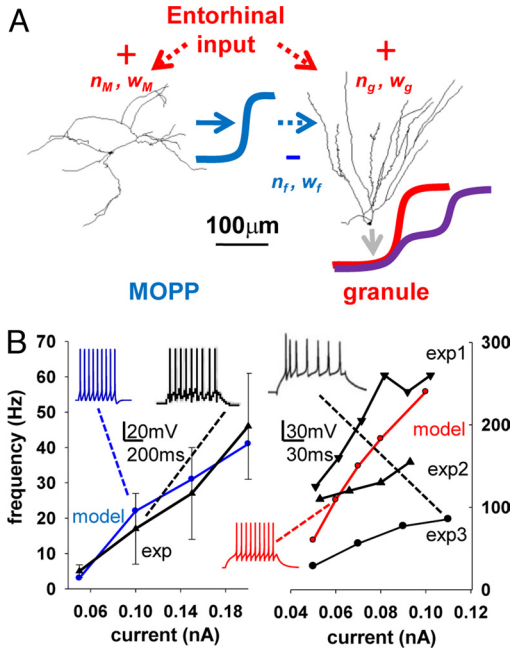

Fig. 1. Basic intrinsic properties of the modeled cells. (*A*) Schematic representation of the FFI model, including an interneuron (MOPP) and a principal (granule) cell. Red arrows identify the external excitatory input to both cells; n_M, w_M, n_g, and w_g represent number and weight of the synapses on the MOPP and granule cell, respectively. The blue line depicts the inhibitory output of the MOPP cell targeting the granule cell dendrites with n_f synapses of weight w_f. The granule cell output is illustrated without (red line) or with (purple line) the MOPP inhibitory input. (*B*) I-f curves of the model MOPP (*Left*, blue) and granule cell (*Right*, red) describing the firing rate response to somatic current injections. Experimental data (black) were replotted from published reports for MOPP cells (20) and for 3 independent studies of granule cells (exp1 (21), exp2 (22), and exp3 (23), respectively). Insets show somatic recordings for both experiments and models at specific current amplitudes.

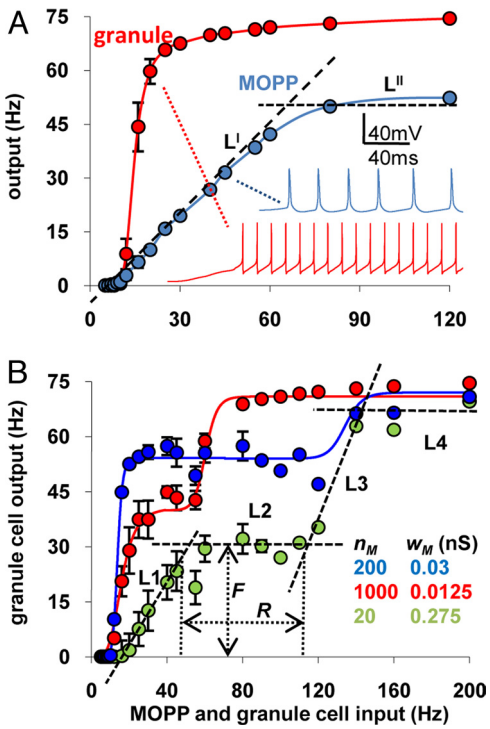

Fig. 2. The number and weight of synaptic inputs on the MOPP cell can modulate the buffering effect of FFI. (*A*) MOPP (blue) and granule cell (red) firing rates as a function of the frequency of excitatory synaptic input (without inhibition on the granule cell). The values for n_M and w_M were 200 and 0.05 nS, respectively. L^I and L^{II} are the lines used to fit the slope and saturation of the MOPP curve. Insets show sample traces for specific cases. (*B*) Granule cell firing rate under different conditions of MOPP activation and determination of *R* and *F*, by fitting the granule cell I/O curve with 4 lines (L1–L4). Error bars are standard deviations ($n = 20$ simulation sets).

Results

Our biophysically and anatomically realistic simulation of FFI in the dentate gyrus is based on compartmental models of a principal (granule) cell and a feed-forward (MOPP) interneuron (Fig. 1*A*). The distribution of passive and active properties in the MOPP and granule cells yielded firing rates as functions of somatic current injection (Fig. 1*B*) in agreement with experimental findings (20–23). The membrane time constant and input resistance of the MOPP cell (15 ms, approximately 200 MΩ) resulting from the model parameters were also within the respective experimental ranges (20). Similarly, the corresponding model values for the granule cells (15 ms, approximately 430 MΩ) were in agreement with empirical observations at physiological temperatures (24, 25).

The I/O curves for the granule cell in the absence of FFI ($n_f = 0$ and/or $w_f = 0$), and for the MOPP cell with a representative combination of number and weight (n_M and w_M) of excitatory synapses, display typical sigmoid shapes (Fig. 2*A*). Altering n_M and/or w_M changed the MOPP cell I/O curve both in terms of signal gain (corresponding to the slope of the linear fit L^I in Fig. 2*A*) and offset (intercept of L^I with the abscissa). In particular, the slope was a tight linear function of the total conductance ($n_M \cdot w_M$), with the same proportionality observed by changing w_M while keeping n_M constant or vice versa ($r > 0.95$). For example, either halving the number of synapses from 200 to 100 (keeping their conductance at 0.05 nS), or halving the conductance to 0.025 nS (while keeping the number at 200) produced an identical reduction of the I/O slope from 0.8 to 0.4. In contrast, halving the number of synapses to 100 while doubling their conductance to 0.1 nS (thus maintaining the same total conductance) maintained the slope value at 0.8 (supporting information (SI) Fig. S1*A*).

The abscissa intercept also was sensitive to the total conductance, but it increased more rapidly with a reduction of the conductance than of the number of synapses. As a result, halving the synaptic number n_M from 200 to 100 increased the intercept from 8 to 14 Hz, but doubling at the same time the conductance w_M from 0.05 to 0.1 nS more than compensated, yielding a net reduction of the intercept to approximately 4.5 Hz (Fig. S1*B*). As a result, increasing the ratio between n_M and w_M, while maintaining their product constant, shifted the curve to the right without altering its slope. In contrast, the MOPP cell saturation frequency (the L^{II} "plateau" of the I/O curve in Fig. 2*A*) was unaffected by either n_M or w_M and remained confined within ± 2% of approximately 50 Hz throughout the above parameter range (Fig. S1*C*). These observations suggest that combined alterations of n_M and w_M could finely tune the resulting I/O curve of granule cells in the presence of FFI.

By adding to the granule cell the FFI signal from the MOPP cell, we investigated whether the granule cell I/O curve could be buffered at intermediate frequencies (compare red and purple curves in Fig. 1*A*). Indeed, as exemplified in Fig. 2*B* for different combinations of n_M and w_M, the I/O function assumes a double sigmoid shape typical of buffer systems. In particular, over a certain input frequency interval (the buffer range *R*), the output firing rate remains nearly constant (at a buffered level *F*). Furthermore, altering the values of n_M and w_M affected both the buffer input range and output firing rate. This suggests a

fundamental physiological role of FFI, namely to normalize the I/O properties of principal cells within values that can be quantitatively controlled by modulating the number and weight of the excitatory synapses on the feed-forward interneuron. Although the main qualitative effect can be obtained from a network of much simpler units (17), the F and R values depend quantitatively on nonlinear interactions within and among active channels and synaptic inputs. A realistic implementation is thus necessary to explore the physiological significance of the parameter ranges.

To ensure that the observed buffering effect of FFI was not a result of specific modeling conditions, we ran multiple control simulations. In particular, we explored the use of synchronous excitatory activation (all synapses activated in phase as opposed to independently of each other), of regular spiking trains (constant interstimulus intervals instead of Poisson distributions), of nonuniform distribution of synaptic frequencies between 0 and 200% of the average "target" value (as opposed to the same input rate for all synapses), and of a fixed spatial distribution of synapses (instead of redistributing the inputs at each simulations). Although the buffered firing rate F varied in each condition, the general buffering effect of FFI was robustly reproduced in all cases: the buffer range R never approached zero and in fact was always greater than in the "base" conditions selected for this study (Fig. S2).

To explore systematically the effects of n_M and w_M on R and F, we varied the number of synapses on the MOPP cell dendrites while holding their weight at different fixed values, and vice versa, we changed the weight while maintaining the synapse number constant. Both the output firing rate (Fig. 3 *A* and *B*) and the input frequency range (Fig. 3 *C* and *D*) of the granule cell buffered I/O curve were well fitted by independent linear functions of n_M and w_M (average r^2: 0.92). The negative slope and left shift of these lines with increasing MOPP cell stimulation indicate that a stronger excitatory input to the FFI interneuron tends to lower the buffered firing rate and to restrict the dynamic range of the buffer. Such dual linear behavior is consistent with a set of 2 second-order equations in 2 variables without quadratic terms:

$$R = a{\cdot}n_M{\cdot}w_M + b{\cdot}n_M + c{\cdot}w_M + d$$

$$F = e{\cdot}n_M{\cdot}w_M + f{\cdot}n_M + g{\cdot}w_M + h,$$

where the slope and intercept of R as a function of n_M at a fixed w_M value are given respectively by $(a{\cdot}w_M{+}b)$ and $(c{\cdot}w_M{+}d)$, and analogous relations hold for each pair of dependent and independent variables. Square error minimization yielded best fitting values for parameters a–h: $a = -16.24$ Hz/nS, $b = -204.05$ Hz, $c = 0.036$ Hz/nS, $d = 189.07$ Hz, $e = -3.92$ Hz/nS, $f = -83.13$ Hz, $g = 0.021$ Hz/nS, $h = 71.35$ Hz. Inspection of these values reveals that the cross and residual terms (a and d in R) are relatively more predominant (compared to b and c) in the equation of the input range than in that of the firing rate.

These results imply that the buffering properties of FFI can be modulated broadly. Specifically, the output firing rate can be equalized to any level between 20% and 80% of the saturation frequency of the principal cell (approximately 70 Hz in this case), and the dynamic range of the neuron can be augmented >10-fold relative to the purely excitatory I/O relationship (from <10 Hz to >100 Hz). Moreover, these two features can be independently controlled by appropriate combinations of the number and weight of excitatory synapses on the interneuron, all within a reasonable biological variation. In particular, to yield a desired pair of values for R and F, the corresponding quantities of n_M and w_M can be computed with the quadratic formula after substitution from the above equations (Fig. 3 *E* and *F*). For example, to obtain a buffered output

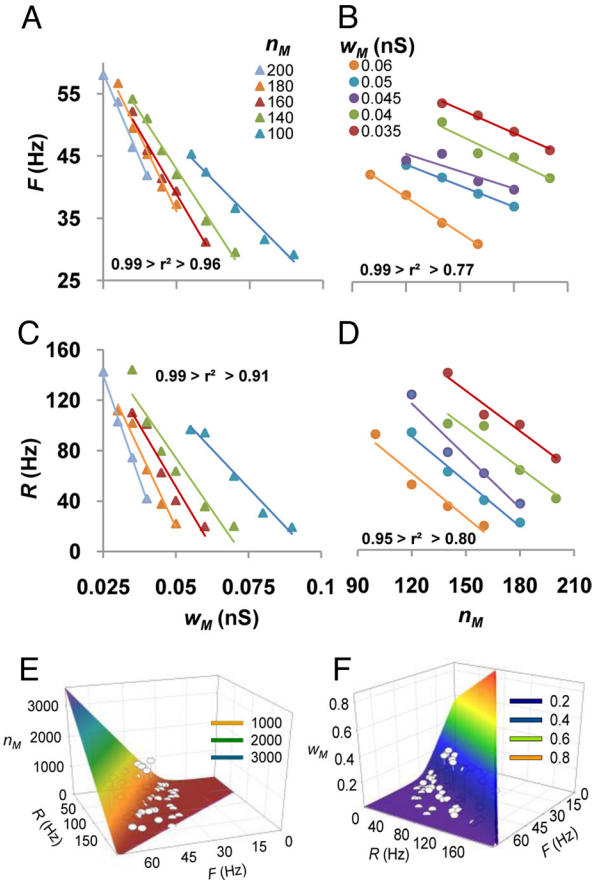

Fig. 3. The buffer range and frequency can be broadly and systematically controlled by the input to the inhibitory neuron. (*A–D*) Independent modulation of the granule cell firing rate F (*Top*) and range R (*Bottom*) as a function of the weight w_M (*Left*) and number n_M (*Right*) of the excitatory synapses on the MOPP cells. (*E–F*) Computed n_M and w_M values to obtain a target pair of F and R values. The quadratic equation has 2 solutions for each pair of F and R (high n_M and low w_M or vice versa), illustrated by corresponding color shades. Dots are fitted data.

firing rate of 25 Hz over an input frequency dynamic range of 20 Hz (corresponding to a stimulation interval of 10–30 Hz), the inhibitory cell should receive 140 synapses of 0.07 nS weight. The output firing rate could be doubled (with the same input frequency range) by changing the synaptic values n_M and w_M to 1600 and 0.0856 nS, respectively. Similarly, the input range could be extended to 40 Hz (10–50 Hz stimulation), without altering the buffered firing frequency, with n_M and w_M values of 18 and 0.335 nS, respectively.

Inhibitory neurons can also inhibit each other (18), potentially decreasing the slope of their I/O curve. To investigate the impact of such possibility on the I/O relation of granule cells, in a variant of the model we substituted the MOPP cell with a randomly connected network of 10 mutually inhibiting interneurons (see *SI Text*). This variation drastically enhanced the buffering effect of FFI (Fig. S3*A Left*) by more than doubling R and progressively lowering F with increasing synaptic coupling (Fig. S3*A Right*).

As synaptic plasticity could also dynamically affect FFI, we explored the effect of short-term depression of the inhibitory contacts (see *SI Text* for details and rationale), using parameters from the experimental literature (26). This mechanism added a temporal dimension to the buffer (Fig. S3*B*). The strong effect observed at stimulation onset was drastically reduced after approximately 250 ms (*Left*), practically disappearing at 500 ms,

with corresponding decay of R and gradual increase of F (*Right*). These simulations thus predict a finite time window for FFI buffering.

Discussion

Ever since their establishment as the fundamental spiking devices in the nervous system, neurons have been recognized for their ability to transform rate-coded information. The I/O relation between the mean firing frequencies of the excitatory synaptic input and axonal output is typically described as a sigmoid function (27), whereas the neuron is nearly silent at input rates below a characteristic offset, then at intermediates input rates increases its firing output with a given slope or gain, finally reaching a plateau at saturation input rates. Synaptic integration and neuronal excitability, and thus the shape of the I/O curve, are affected by many factors, including dendritic morphology, passive and active membrane properties, and the spatiotemporal input patterns.

The all-or-none properties of axonal spiking and the presence of active dendritic channels can yield a steep I/O sigmoid (28) with limited dynamic range. The resulting nearly bimodal behavior may severely compromise information coding, as minimal input fluctuations within the expected natural variability could cause neuronal output to jump between silence and maximum firing rate. Network simulations of feed-forward excitation, notoriously susceptible to falling into bistable activity (29), are often fixed with external algorithms that impose hard constraints on average and instantaneous firing rates (30). These solutions are meant to capture underlying inhibitory dynamics, but the actual biological mechanism allowing the extensive feed-forward excitatory networks in the cortex to operate continuously over a broad frequency range is unknown.

Our results demonstrate that FFI may allow the continuous control of the circuit I/O, providing a soft switch between essentially digital and analog rate-code. The qualitative transition of the traditional synaptic integration mode to a buffer system greatly enhances the robustness of the response to noisy stimuli. This could be crucial in brain regions prone to epileptic activity such as the hippocampus, where excitability is finely regulated by multiple inhibitory mechanisms (31). The dentate gyrus, entry point of the hippocampal circuit, is especially sensitive, and disruption of its inhibitory efficacy may cause the aberrant activity observed after brain injury (32). Buffering the granule cell I/O may also be essential to spatial coding of place cells (*SI Text*). A prominent FFI circuit is also present in CA1, where pyramidal cells receive GABAergic input corresponding to each of the 2 main excitatory afferents, namely Schaffer collateral from CA3 (33) and perforant pathway from the entorhinal cortex (34). Interestingly, in CA1 pyramidal cells the relative contribution to network activity of feed-forward and feedback inhibition (respectively from radiatum and alveus interneuron) depends on the input frequency at the afferent fibers (9).

The proposed FFI mechanism enables the quantitative and independent modulation of the buffered I/O properties, input range, and output firing rate, by synaptic circuit fine tuning. Although we only presented analyses of the simulations that altered the excitatory input to the interneuron (n_M and w_M), similar results can be obtained by varying the number and weight of the inhibitory contacts on the principal cell (n_f and w_f). Both of these connection types are dynamically regulated in the cortex through a variety of short- and long-term plasticity mechanisms (26, 35). Thus, plastic synaptic changes could rapidly regulate both the buffered firing rate output (F) and the corresponding range of input frequency (R), while maintaining the robustness of the buffer system (Fig. S3).

Our computational model, designed from a parsimonious set of biophysically and anatomically plausible conditions, provided a ''proof by construction'' for this novel potential role of FFI. The goal was to test whether the hypothesized buffer function could be achieved in a biologically relevant interval of frequencies with realistic connectivity. From this perspective, the lack of other biophysical details such as Ca^{2+} dynamics or homeostatic plasticity is a feature, not a limitation. The model was validated with available experimental data most pertinent to the I/O relationship (the I-f curves) but did not attempt to recreate faithfully all aspects of MOPP and granule cell electrophysiology or to reproduce phenomena not directly affecting mean firing rate. In fact, except for the selection of an anatomically well-characterized FFI circuit (the entorhinal-MOPP-granule cell system), these results might be representative of other FFI circuits throughout the cortex and other brain regions. The Na^+ and K^+ channels in our model are ubiquitous components of active membranes, ultimately determining neuronal excitability and thus the I/O relationship. At the same time, the buffering ability of FFI demonstrated here could be further modulated by other membrane properties and subcellular mechanisms, such as the up/down-regulation of the interneuron K^+ conductances (36). Similarly, the stimulation characteristics could also play a role: to a first approximation, increasing the synchrony of synaptic activation corresponds to grouping synapses together (37), i.e., raising

Table 1. Morphometric properties[a]

	MOPP (N = 12)			Granule (N = 19)		
	n257	$\mu \pm \sigma$	Min–Max	n500	$\mu \pm \sigma$	Min–Max
# Dendritic trees	4	3.6 ± 1.1	2–5	2	1.9 ± 1.1	1–4
# Branches	147	126 ± 58.6	63–283	35	37.4 ± 11.3	23–67
Width, μm	585	662 ± 206	309–1029	326	300 ± 72.2	182–518
Height, μm	642	501 ± 196	257–961	270	260 ± 54.9	159–401
Depth, μm	24.8	41.3 ± 20.8	20.3–86	56.1	208 ± 94.9	31–377
Avg. diameter, μm	0.6	0.7 ± 0.2	0.5–1.3	0.5	0.8 ± 0.2	0.5–1.2
Total length, μm	11994	10455 ± 4802	2745–19053	3025	4058 ± 959	2298–6060
Max eucl. dist., μm	437	508 ± 104	312–678	400	385 ± 39.6	327–456
Max path dist., μm	1618	1182 ± 443	421–2161	419	482 ± 55.1	399–597
Max branch order	20	15 ± 6.1	7–27	6	5.7 ± 1	3–7
Partition asymmetry	0.5	0.5 ± 0.1	0.4–0.7	0.6	0.5 ± 0.1	0.2–0.6
Bifurcation angle, deg	80.8	76.8 ± 8.8	66.3–90.2	47.8	43.4 ± 6.6	29.8–53.2

[a]All NeuroMorpho.Org reconstructions that belonged to the same classes as n257 and n500 (12 MOPP and 19 granule cells) were used in the analysis. MOPP cells include both axons and dendrites (axons were excluded in subsequent modeling); only dendrites were reconstructed in these granule cells.

Table 2. Passive and active properties

	MOPP	Granule
Resting potential, mV	−55	−74
R_m, KΩ·cm^2	15	6
C_m, μF/cm^2	1	2.5
R_a, Ω·cm	150	200
Input impedance, MΩ	199.6	433
g_{Na} soma/dend, pS/μm^2	800/160	2000/666
g_{K_DR} soma/dend, pS/μm^2	100/20	
g_{K_A} soma/dend, pS/μm^2	200/40	
g_{K_f}, pS/μm^2		600

their weight (w) while lowering their number (n), consistent with the doubling of R in Fig. S2.

The simple conditions selected in this study point to the generality of the FFI buffer function that might dramatically increase the computational power of neuronal integration. An experimentally testable prediction of this model is that an intermediate plateau could be observed in the I/O relationship of neurons controlled by FFI and that this deviation from a sigmoid curve would be eliminated by blocking GABAergic conduction. Preliminary evidence may be found in recent experimental data (38, 39). However, the different conditions of these approaches (fixed pharmacological inhibition or indirect measure of firing rate) invite caution. Stronger experimental tests could involve organotypic slice cultures of entorhinal cortex and dentate gyrus to isolate the feed-forward component (40).

Different populations of interneurons often coexist in a given brain circuit (2). Thus, more than one class of feed-forward cells could independently target the same population of principal neurons, each with distinct synaptic parameters (e.g., number and weights of excitatory synapses on the interneuron). This would result in multiple buffer effects on the I/O curve of the principal cells, each with its own dynamic range R and buffered firing rate F. The example illustrated in Fig. S4, resembling the pH titration curve of a weak polyacid, was created by using for each of the neurons a generic I/O sigmoid (the integral form of the normal distribution, or error function), emphasizing that this phenomenon reflects a general computational property of FFI architectures (17) and not a specific combination of biophysical parameters.

Methods

The 3D morphological reconstructions of the 2 cells were downloaded from Turner's collection (41) of the public NeuroMorpho.Org database (42) (http://neuromorpho.org), namely *n500* (granule) and *n257* (MOPP). The morphometric parameters of these neurons were representative of their respective classes (Table 1). The NEURON models files and a simulation script are publicly available on the ModelDB database (http://senselab.med.yale.edu). More details are described in *SI Text*.

Passive and active properties in both cells (Table 2) matched empirical values if reported (22, 43), or were set to obtain I-f curves consistent with available experimental data (20–23) (Fig. 1*B*). This selection aimed at the simplest biophysical models suitable to explore the I/O relationships in terms of mean firing rate. For the sake of parsimony, Ca^{2+}, Ca^{2+}-dependent, and other slow conductances involved in spike adaptation, after-hyperpolarization, depolarizing after-potential, and other postspike events (43) were not included. The large difference in capacitance between the 2 cells accounts for the contribution to membrane surface area of dendritic spines, which are dense in granule cells (44), but not in MOPP cells (18).

Granule and MOPP cells received a barrage of excitatory synaptic stimulation from the same (''entorhinal'') source (red arrows in Fig. 1*A*). In both cells, these inputs were stochastically distributed on the dendrites in the outer two-thirds of the molecular layer, corresponding to the perforant pathway. Unless otherwise noted, each synapse received an asynchronous train of irregular stimuli at the same mean frequency. In particular, interspike intervals were independently sampled from a Poisson distribution matching the target mean frequency, and the phase (i.e., the first activation time) of each synapse was uniformly sampled between zero and the interspike interval. The granule cell was also targeted by inhibitory synapses from the MOPP cell (blue dotted arrow in Fig. 1*A*) in the same dendritic zones.

Excitatory (AMPA and NMDA) and inhibitory ($GABA_A$) synapses were modeled using double exponential time courses. Raise and decay time constants, number of synapses, dendritic location, peak conductance, and reversal potential (Table 3) were consistent with available experimental data (*SI Text*). To test if model and results were representative of a more general phenomenon not restricted to the rodent dentate gyrus, we also tried a broader range of values. Such exploratory simulations indicated that the main finding was robustly reproducible with several alternative combinations. For example, buffering is observed also in the absence of NMDA conductances in granule cells. Therefore, the selected simulation parameters should be interpreted as a proof of principle and not in the limiting sense.

The output of the inhibitory neuron (schematized by the blue sigmoid in Fig. 1*A*) and its effect on the granule cell could be modulated by several parameters, including the number and weight of excitatory inputs on the MOPP cell (n_M and w_M, respectively) and of its feed-forward outputs (n_f and w_f). In the hypothesized FFI mechanism described in the Introduction, the ratio between excitatory and inhibitory input to the granule cell ($n_g \cdot w_g / n_f \cdot w_f$) must match the MOPP cell gain, i.e., the slope of the I/O curve of the interneuron between offset and saturation. Since the numbers of excitatory and inhibitory synapses on the granule cell (n_g and n_f) were fixed to the same constant number (2000), only n_M and w_M remained as free parameters. To study the I/O characteristics of the circuit (Fig. 1*A*), simulations were run for several combinations of n_M and w_M, keeping in all cases n_g and w_g constant (Table 3). For each combination, the output firing frequency of the granule cell was computed as a function of the excitatory input frequency over a simulation period sufficient to record 10 or more spikes at each input frequency. Results were averaged over 20 simulations, stochastically resampling in each case the location and initial activation time (phase) of individual synapses.

The interneuron gain was computed by least square error fitting of the MOPP cell I/O results with a 3-parameter function defined as the minimum between a line, determining the slope, and a constant corresponding to the saturation frequency (Fig. 2*A*). Similarly, the buffered firing rate F and the buffering range R were found by best fit of the granule cell I/O data with a 6-parameter function consisting of 2 linear components and 2 constants, corresponding to the intermediate plateau and to the saturation frequency (Fig. 2*B*).

Separate simulations modeled short-term depression of GABAergic synapses (26) by monotonically decreasing w_f with each activation, plateauing at the 5th to 40% of the initial value.

Table 3. Synaptic properties

Cell	Distribution (distance from soma)	Type	Number (n_x)	Reversal potential	Peak conductance (w_x, in nS)	Raise/decay time, ms
MOPP	>300 μm	AMPA	14–1000	0 mV	0.0075–0.3	0.5/3
Granule	>200 μm	NMDA	2000	0 mV	0.02	0.5/10
		AMPA	2000	0 mV	0.04	0.5/3
	>200 μm	GABA	2000	−80 mV	0.012–0.039[a]	0.5/10

[a]This value was adjusted to match the ratio between the excitatory conductance on the granule cell and the gain of the MOPP (the slope of the linear component of its I/O curve between offset and saturation).

In another simulation set, 10 MOPP cells, each receiving the same random excitatory input (w_M and n_M), were interconnected with 200 inhibitory synapses stochastically sampled (with repetition) among all possible pairs (*SI Text*).

ACKNOWLEDGMENTS. The authors are grateful to Drs. John Baker and Alexander Komendantov for useful discussion. This work was supported in part by National Institutes of Health R01 grants AG25633 and NS39600.

1. Jonas P, et al. (2004) Interneuron diversity series: Fast in, fast out–temporal and spatial signal processing in hippocampal interneurons. *Trends Neurosci* 27:30–40.
2. Klausberger T, Somogyi P (2008) Neuronal diversity and temporal dynamics: The unity of hippocampal circuit operations. *Science* 321:53–57.
3. Holt GR, Koch C (1997) Shunting inhibition does not have a divisive effect on firing rates. *Neural Comput* 9:1001–1013.
4. Mitchell SJ, Silver RA (2003) Shunting inhibition modulates neuronal gain during synaptic excitation. *Neuron* 38:433–445.
5. Gupta A, Wang Y, Markram H (2000) Organizing principles for a diversity of GABAergic interneurons and synapses in the neocortex. *Science* 287:273–278.
6. Ascoli GA, et al. (2008) Petilla terminology: Nomenclature of features of GABAergic interneurons of the cerebral cortex. *Nat Rev Neurosci* 9:557–568.
7. McBain CJ, Fisahn A (2001) Interneurons unbound. *Nat Rev Neurosci* 2:11–23.
8. Mittmann W, Chadderton P, Häusser M (2004) Neuronal microcircuits: Frequency-dependent flow of inhibition. *Curr Biol* 14:R837–R839.
9. Wierenga CJ, Wadman WJ (2003) Excitatory inputs to CA1 interneurons show selective synaptic dynamics. *J Neurophysiol* 90:811–821.
10. Thomson AM, Lamy C (2007) Functional maps of neocortical local circuitry. *Front Neurosci* 1:19–42.
11. Pinto A, Fuentes C, Paré D (2006) Feedforward inhibition regulates perirhinal transmission of neocortical inputs to the entorhinal cortex: Ultrastructural study in guinea pigs. *J Comp Neurol* 495:722–734.
12. Finch DM, Tan AM, Isokawa-Akesson M (1988) Feedforward inhibition of the rat entorhinal cortex and subicular complex. *J Neurosci* 8:2213–2226.
13. Buzsáki G (1984) Feed-forward inhibition in the hippocampal formation. *Prog Neurobiol* 22:131–153.
14. Haberly LB, Bower JM (1984) Analysis of association fiber system in piriform cortex with intracellular recording and staining techniques. *J Neurophysiol* 51:90–112.
15. Pouille F, Scanziani M (2001) Enforcement of temporal fidelity in pyramidal cells by somatic feed-forward inhibition. *Science* 293:1159–1163.
16. Trevelyan AJ, Sussillo D, Yuste R (2007) Feedforward inhibition contributes to the control of epileptiform propagation speed. *J Neurosci* 27:3383–3387.
17. Ascoli GA, Atkeson JC (2005) Incorporating anatomically realistic cellular-level connectivity in neural network models of the rat hippocampus. *BioSystems* 79:173–181.
18. Han ZS, et al. (1993) A high degree of spatial selectivity in the axonal and dendritic domains of physiologically identified local-circuit neurons in the dentate gyrus of the rat hippocampus. *Eur J Neurosci* 5:395–410.
19. Ceranik K, et al. (1997) A novel type of GABAergic interneuron connecting the input and the output regions of the hippocampus. *J Neurosci* 17:5380–5394.
20. Mott DD, et al. (1997) Interneurons of the dentate-hilus border of the rat dentate gyrus: Morphological and electrophysiological heterogeneity. *J Neurosci* 17:3990–4005.
21. Scharfman HE (1995) Electrophysiological diversity of pyramidal-shaped neurons at the granule cell layer/hilus border of the rat dentate gyrus recorded in vitro. *Hippocampus* 5:287–305.
22. Gao TM, Howard EM, Xu ZC (1998) Transient neurophysiological changes in CA3 neurons and dentate granule cells after severe forebrain ischemia in vivo. *J Neurophysiol* 80:2860–2869.
23. Yun SH, et al. (2006) Amyloid-beta1–42 reduces neuronal excitability in mouse dentate gyrus. *Neurosci Lett* 403:162–165.
24. Spruston N, Johnston D (1992) Perforated patch-clamp analysis of the passive membrane properties of three classes of hippocampal neurons. *J Neurophysiol* 67:508–529.
25. Isokawa M (1997) Membrane time constant as a tool to assess cell degeneration. *Brain Res Brain Res Protoc* 1:114–116.
26. Hefft S, Kraushaar U, Geiger JRP, Jonas P (2002) Presynaptic short-term depression is maintained during regulation of transmitter release at a GABAergic synapse in rat hippocampus. *J Physiol 539* 1:201–208.
27. Bartesaghi R, Migliore M, Gessi T (2006) Input-output relations in the entorhinal cortex-dentate-hippocampal system: Evidence for a non-linear transfer of signals. *Neuroscience* 142:247–265.
28. Reyes A (2001) Influence of dendritic conductances on the input-output properties of neurons. *Annu Rev Neurosci* 24:653–675.
29. Levy WB, Deliç, H, Adelsberger-Mangan DM (1999) The statistical relationship between connectivity and neural activity in fractionally connected feed-forward networks. *Biol Cybern* 80:131–139.
30. O'Reilly RC, Munakata Y (2000) in *Computational Explorations in Cognitive Neuroscience: Understanding the Mind by Simulating the Brain* (MIT Press, Cambridge, MA).
31. Sloviter RS (1991) Feedforward and feedback inhibition of hippocampal principal cell activity evoked by perforant path stimulation: GABA-mediated mechanisms that regulate excitability in vivo. *Hippocampus* 1:31–40.
32. Bonislawski DP, Schwarzbach EP, Cohen AS (2007) Brain injury impairs dentate gyrus inhibitory efficacy. *Neurobiol Dis* 25:163–169.
33. Cope DW, et al. (2002) Cholecystokinin-immunopositive basket and Schaffer collateral-associated interneurones target different domains of pyramidal cells in the CA1 area of the rat hippocampus. *Neuroscience* 109:63–80.
34. Kunkel DD, Lacaille JC, Schwartzkroin PA (1988) Ultrastructure of stratum lacunosum-moleculare interneurons of hippocampal CA1 region. *Synapse* 2:382–394.
35. McBain CJ, Maccaferri G (1997) Synaptic plasticity in hippocampal interneurons? A commentary. *Can J Physiol Pharmacol* 75:488–494.
36. Rush ME, Rinzel J (1995) The potassium A-current, low firing rates and rebound excitation in Hodgkin-Huxley models. *Bull Math Biol* 57:899–929.
37. Li X, Ascoli GA (2008) Effects of synaptic synchrony on the neuronal input-output relationship. *Neural Comput* 20:1717–1731.
38. Mehaffey WH, et al. (2005) Deterministic multiplicative gain control with active dendrites. *J Neurosci* 25:9968–9977.
39. Carvalho TP, Buonomano DV (2009) Differential effects of excitatory and inhibitory plasticity on synaptically driven neuronal input-output functions. *Neuron* 61:774–785.
40. Del Turco D, Deller T (2007) Organotypic entorhino-hippocampal slice cultures–a tool to study the molecular and cellular regulation of axonal regeneration and collateral sprouting in vitro. *Methods Mol Biol* 399:55–66.
41. Cannon RC, et al. (1998) An on-line archive of reconstructed hippocampal neurons. *J Neurosci Methods* 84:49–54.
42. Ascoli GA (2006) Mobilizing the base of neuroscience data: The case of neuronal morphologies. *Nat Rev Neurosci* 7:318–324.
43. Aradi I, Holmes WR (1999) Role of multiple calcium and calcium-dependent conductances in regulation of hippocampal dentate granule cell excitability. *J Comput Neurosci* 6:215–235.
44. Desmond NL, Levy WB (1985) Granule cell dendritic spine density in the rat hippocampus varies with spine shape and location. *Neurosci Lett* 54:219–224.